Observation and study of the Higgs boson candidate in the diphoton decay channel with the ATLAS detector

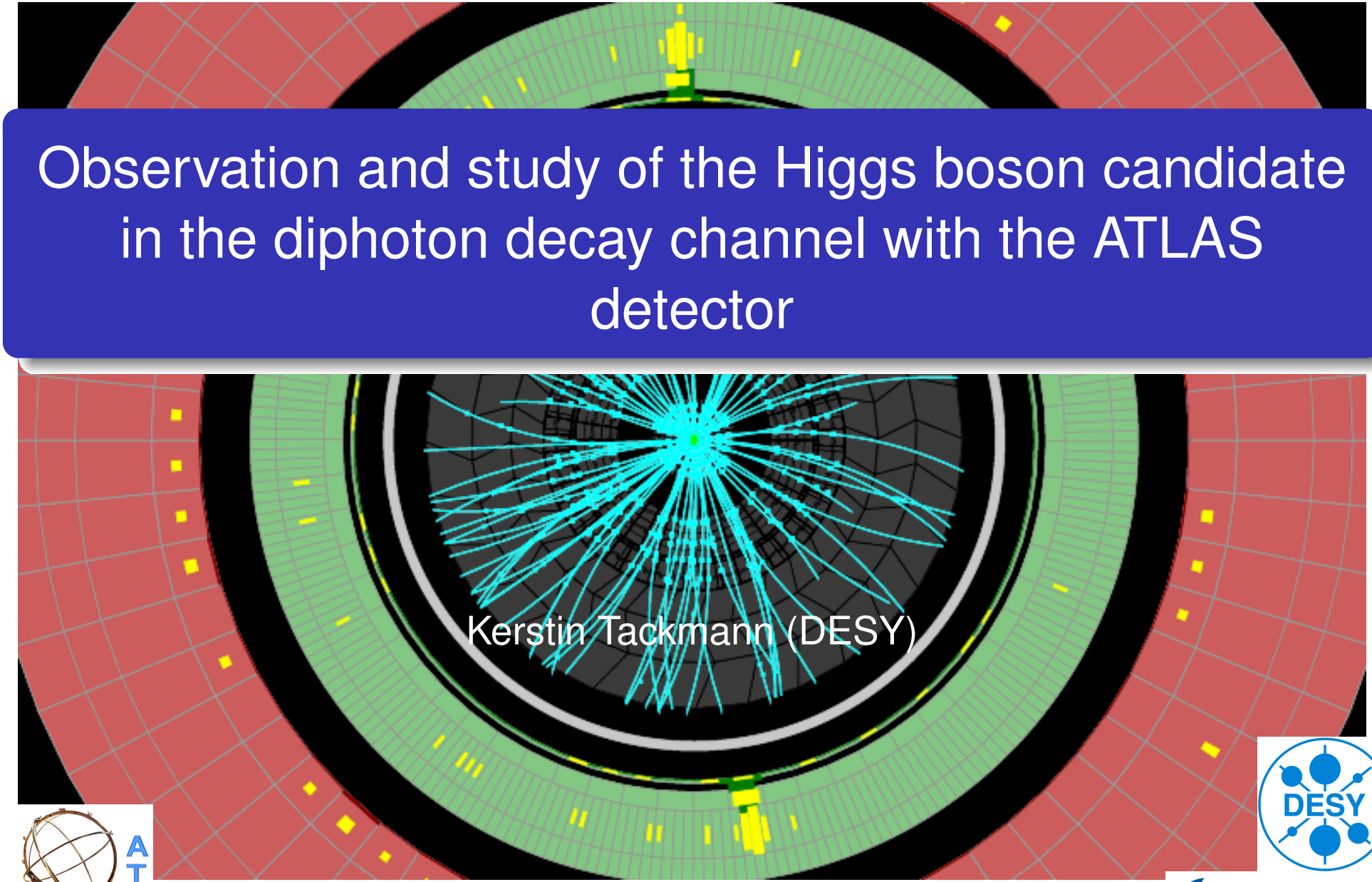

Kerstin Tackmann (DESY)

DPG Frühjahrstagung – March 7, 2013 – Dresden

New particle discovery @ ATLAS and CMS

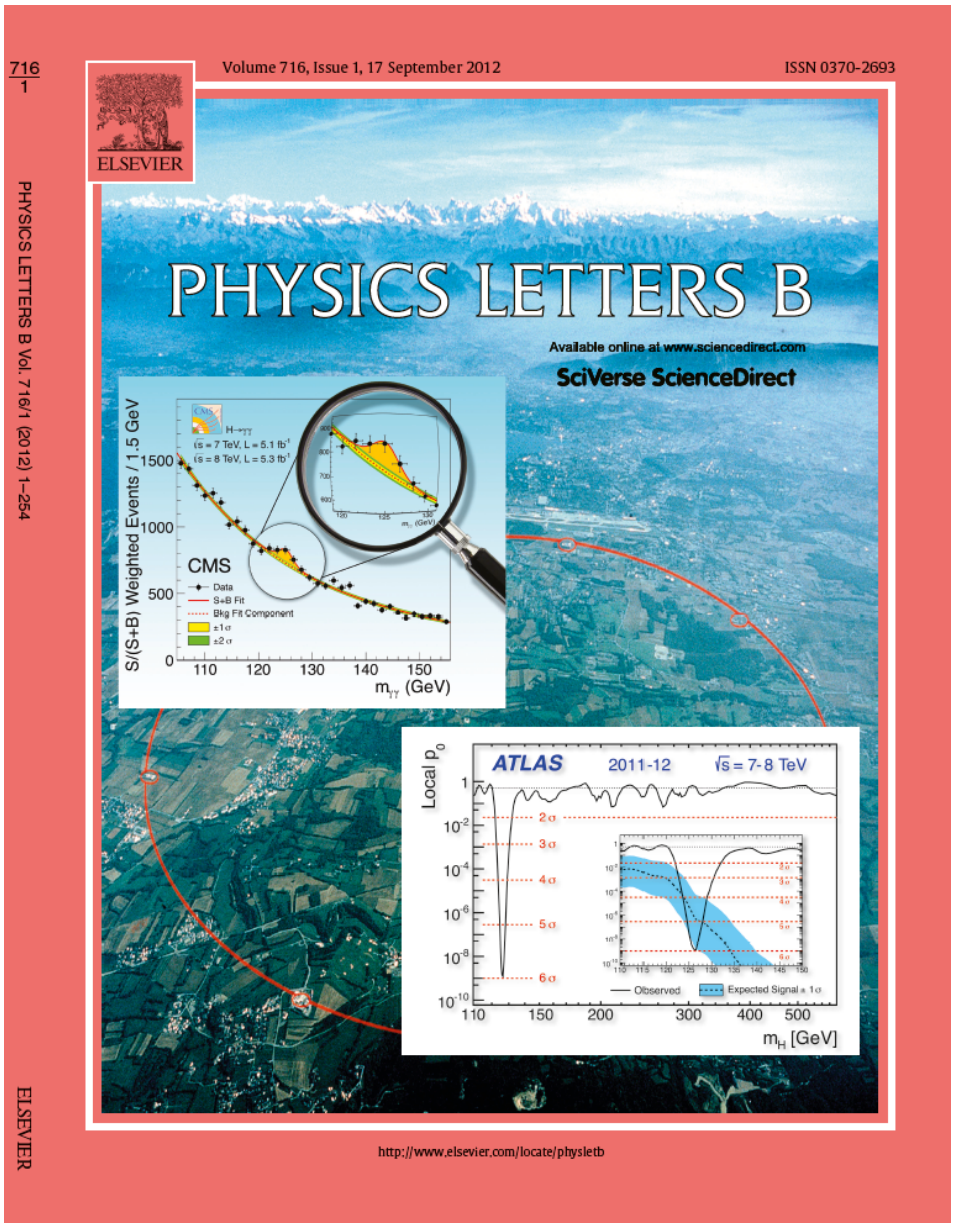

Summer 2012

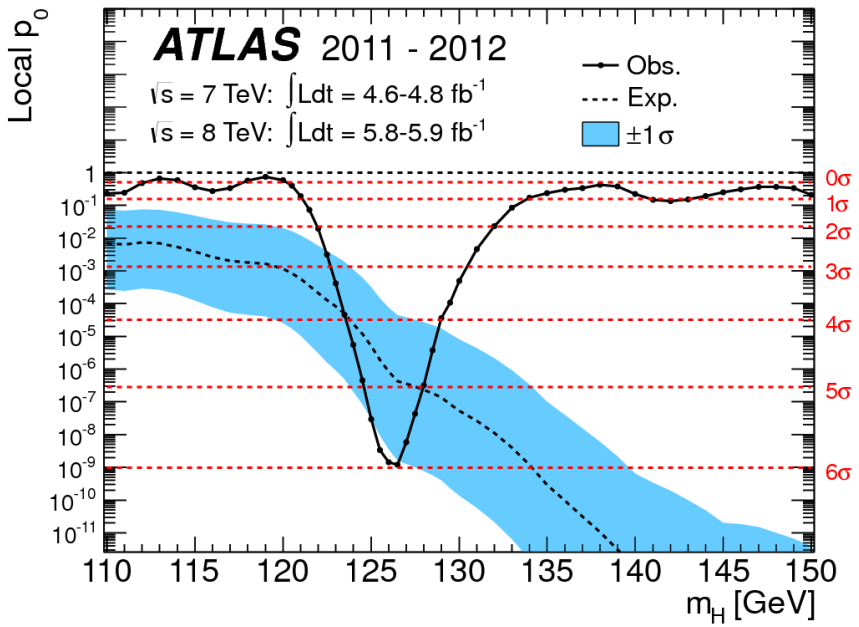

New boson discovered in $\gamma\gamma$, ZZ and WW decays

$5.9\,\sigma$ significance (at that time)

Now: study of properties

See Karl Jakobs' talk yesterday

Higgs boson production at the LHC

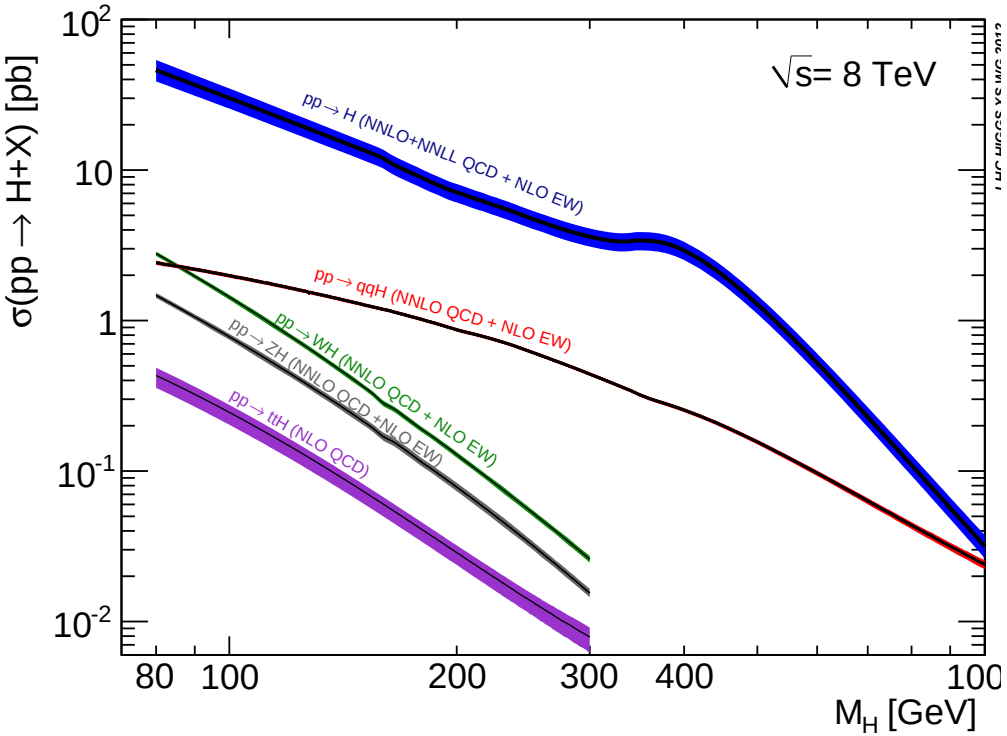

Gluon fusion $19.5\,\mathrm{pb}$

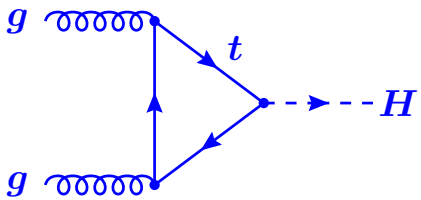

Vector boson fusion $1.6\,\mathrm{pb}$

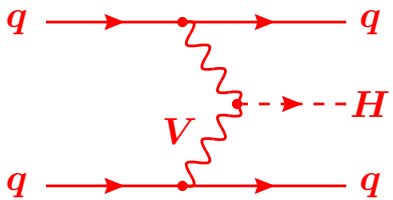

Associated production with $t\bar{t}$ $0.1\,\mathrm{pb}$

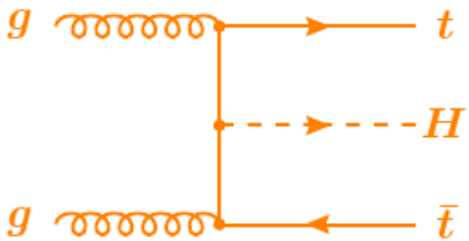

Associated production $1.1\,\mathrm{pb}$

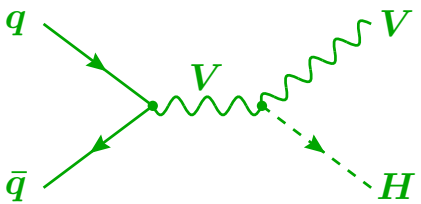

SM Higgs boson decays

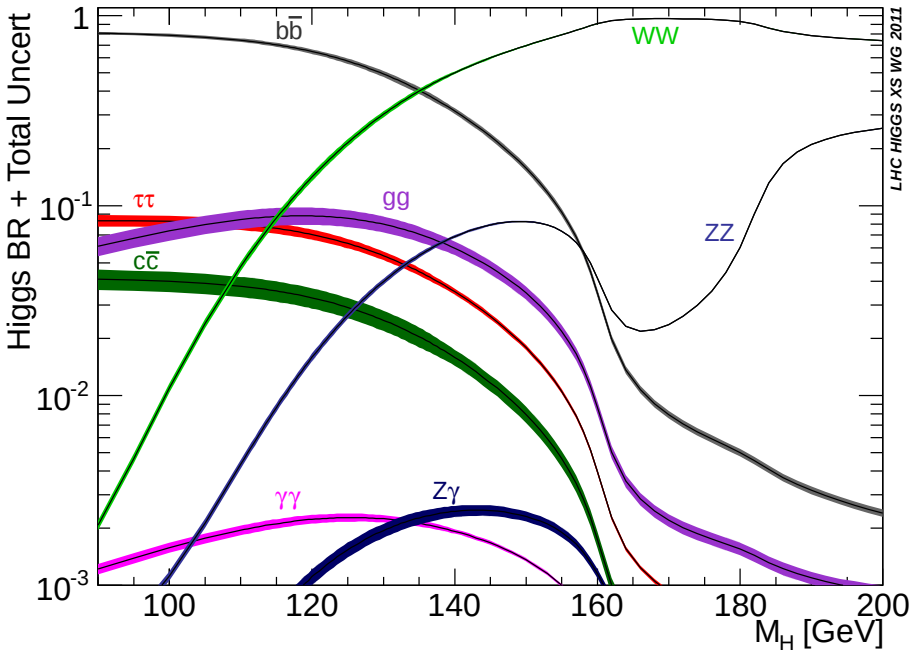

Higgs boson couples to mass

Decay branching fractions @ $m_H = 125\,\mathrm{GeV}$

$H \to b\bar{b}$	57.7%
$H \to WW$	21.5%
$H \to \tau\tau$	6.3%
$H \to ZZ$	2.6%
$H \to \gamma\gamma$	0.23%

$H \to \gamma\gamma$: Comparably simple final state: 2 energetic isolated photons

Large event yield despite low branching fractions expect 475 signal events in current dataset

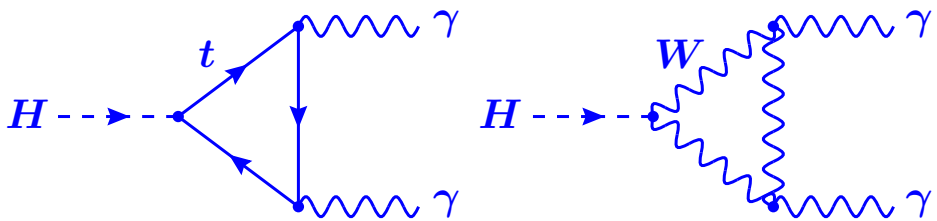

Luminosity and running conditions

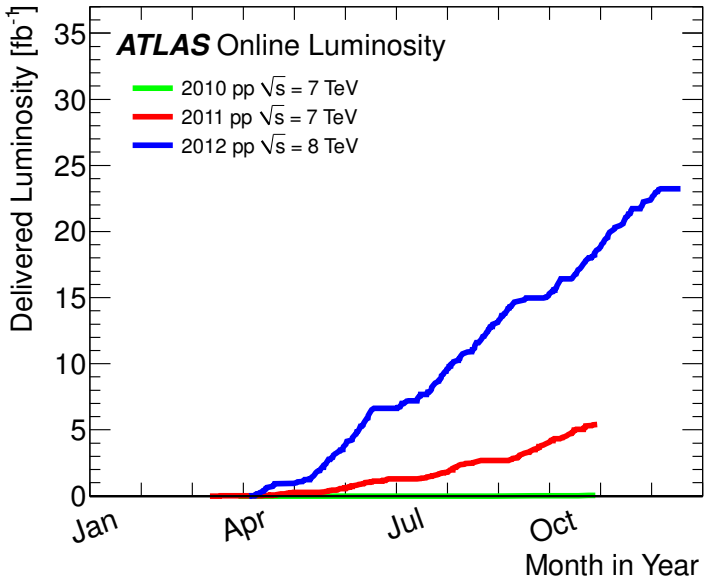

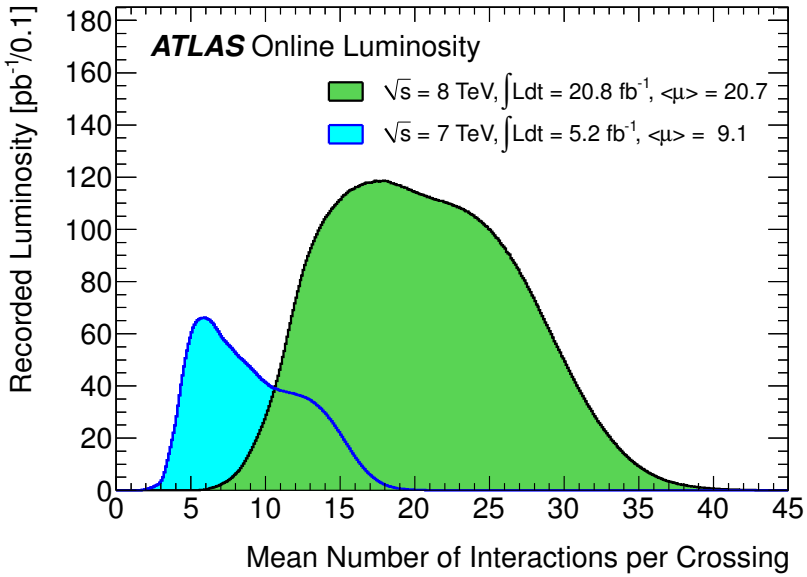

- Outstanding LHC performance: LHC delivered $\sim 6\,\mathrm{fb}^{-1}$ @ $7\,\mathrm{TeV}$ and $\sim 23\,\mathrm{fb}^{-1}$ @ $8\,\mathrm{TeV}$
- Large rise in instantaneous luminosity from $2 \times 10^{32} \rightarrow 7.7 \times 10^{33}$
- Taken with $50\,\mathrm{ns}$ bunch spacing and up to almost 40 interactions/bunch crossing
- Large luminosity comes at the cost of high pileup ($\rightarrow$ many proton-proton collisions overlaid in the detector), challenge to trigger, reconstruction and analysis

Photon reconstruction and identification

- Photon reconstruction from clusters in LAr calorimeter and conversion vertices in Inner Detector
- Need powerful jet-rejection to suppress dominant background ($\mathcal{O}(10^4)$)

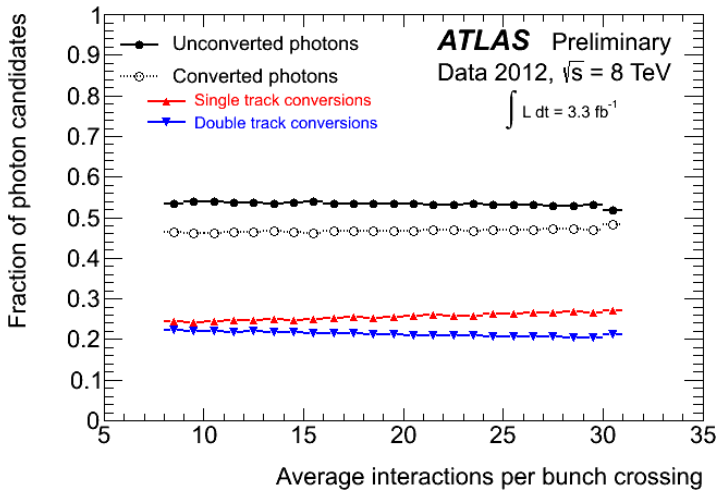

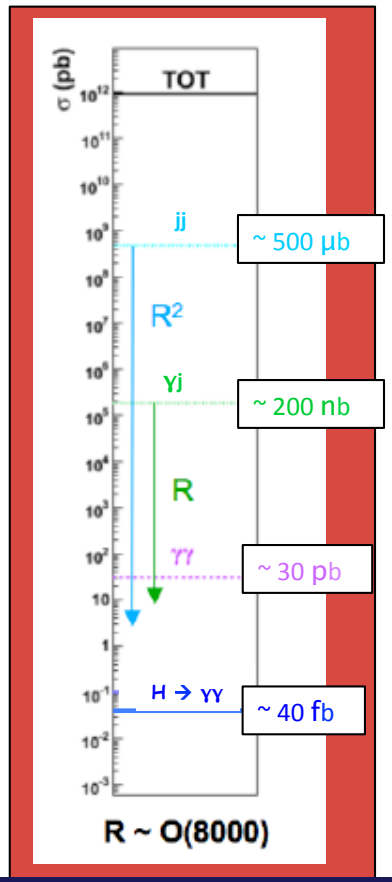

Shower-shaped based photon identification

- $7\,\mathrm{TeV}$: Neural network
- $8\,\mathrm{TeV}$: Rectangular cuts

85% to $> 95\%$ efficient (for isolated photons)

Combined with calorimeter and track isolation requirements

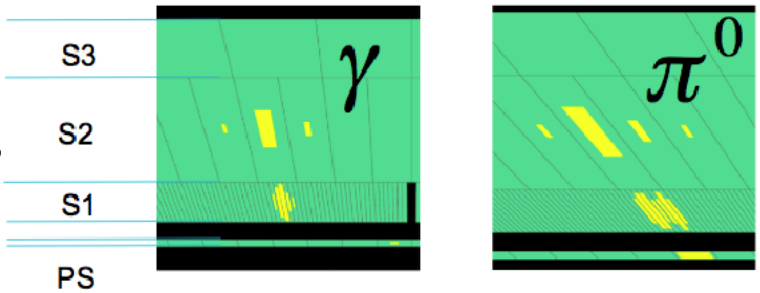

Shower shapes in finely segmented (first layer of) calorimeter

Photon identification and sample composition

Photon identification efficiency (for isolated photons) measured with $Z \to \ell^+\ell^-\gamma$, $Z \to e^+e^-$, id and isolation sideband method

$\mathbf{2.4\%}$ uncertainty on expected signal yield (factor 2 improvement over Dec 2012!)

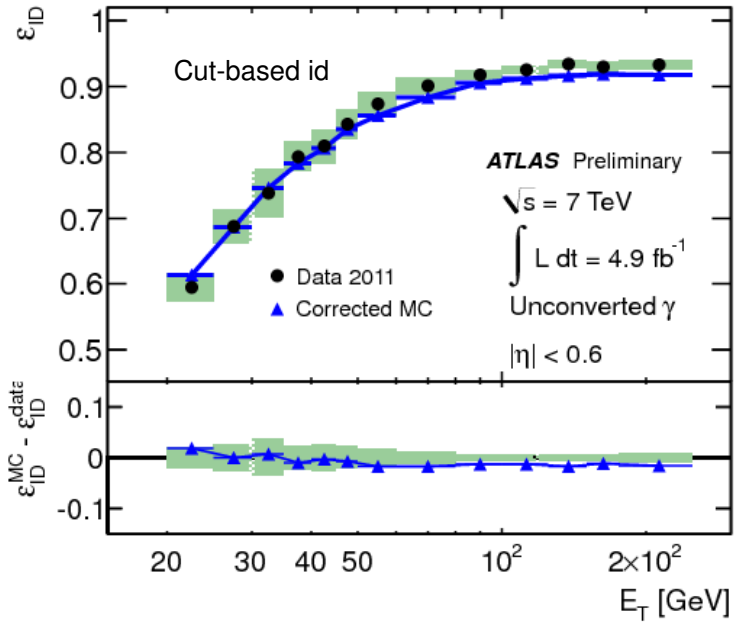

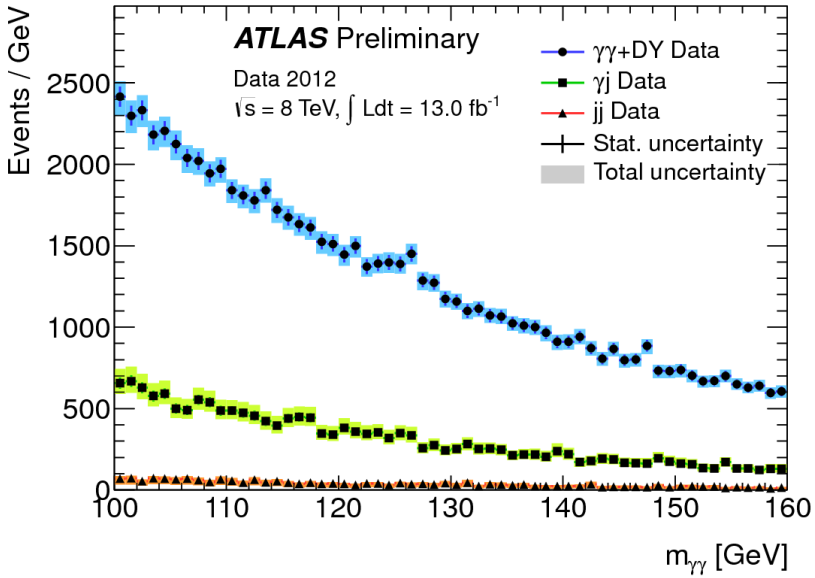

After photon identification and isolation

- $\mathbf{75\%}$ $\gamma\gamma$ events
- $\mathbf{22\%}$ γ jet events
- $\mathbf{3\%}$ jet jet events

Not used directly in analysis, but to monitor photon identification performance and for detailed background shape studies

Energy calibration and invariant mass resolution

$$m_{\gamma\gamma}^2 = 2E_1E_2(1-\cos\alpha)$$

- MC-based calibration improved with energy scale and resolution corrections based on $Z \to e^+e^-$, $W \to e\nu$, $J/\Psi \to e^+e^-$
- Energy scale at m_Z known to between 0.3% to 0.45%
- Energy response of the calorimeter is stable over time and varying pileup conditions at the level of 0.1%
- Understanding of photon energy scale requires understanding of inner detector material budget

  Cross checked with photon conversions, hadronic interactions, $e^{\pm}$ shower shapes and E/p, ...

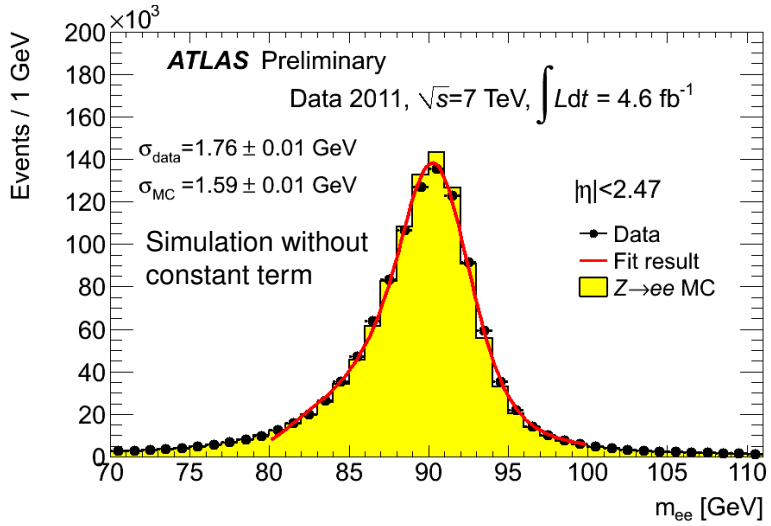

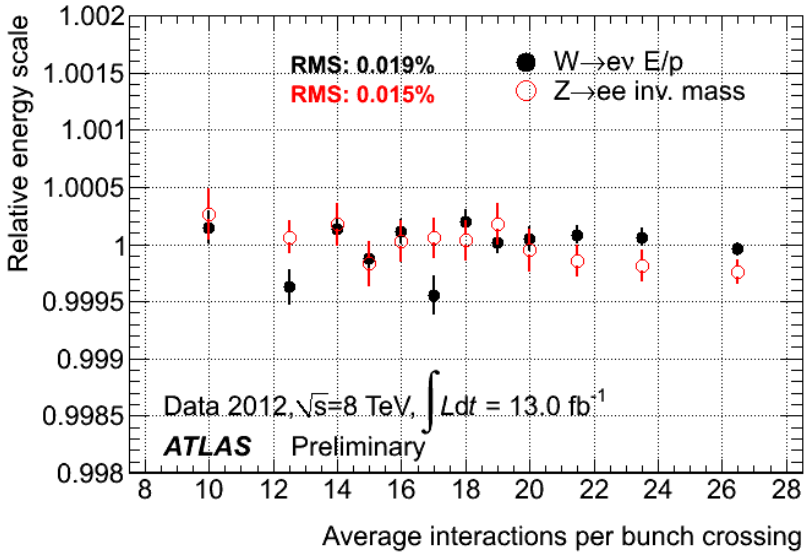

Energy calibration and invariant mass resolution

$$m_{\gamma\gamma}^2 = 2E_1E_2(1-\cos\alpha)$$

- MC-based calibration improved with energy scale and resolution corrections based on $Z \to e^+e^-$, $W \to e\nu$, $J/\Psi \to e^+e^-$
- Energy scale at m_Z known to between 0.3% to 0.45%
- Energy response of the calorimeter is stable over time and varying pileup conditions at the level of 0.1%
- Understanding of photon energy scale requires understanding of inner detector material budget

  Cross checked with photon conversions, hadronic interactions, $e^{\pm}$ shower shapes and E/p, ...

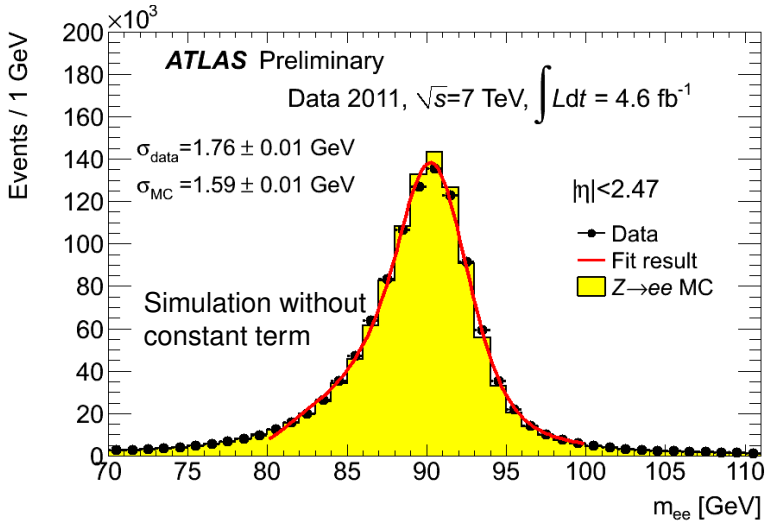

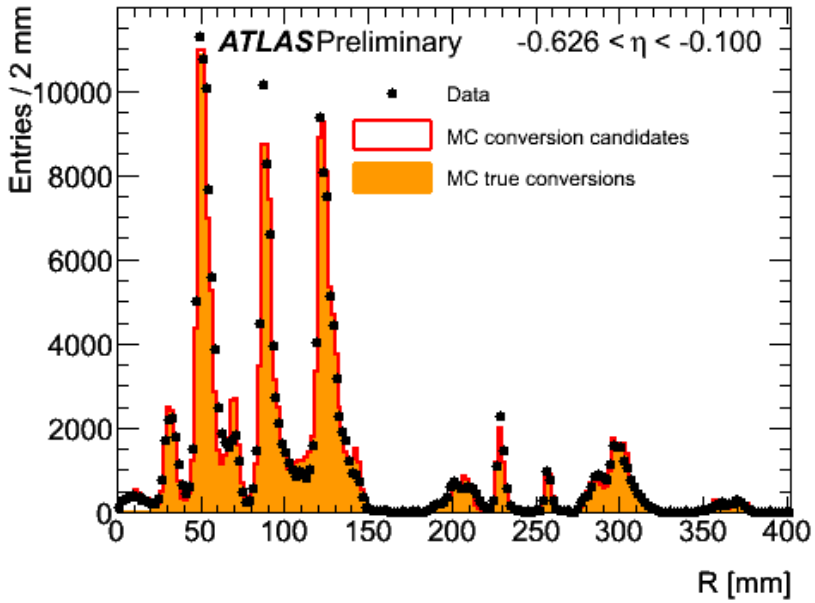

Photon pointing and primary vertex selection

$$m_{\gamma\gamma}^2 = 2E_1E_2(1-\cos\alpha)$$

Improve photon angle measurement using neural network ($8\,\mathrm{TeV}$) based on

- Photon pointing
  - ⋆ Photon direction measured from calorimeter using longitudinal segmentation
  - ⋆ Position of conversion vertex for converted photons (with Si hits)
- $\sum p_T^2$, $\sum p_T$ (over tracks) and angular balance in ϕ between tracks and diphoton system

→ Contribution of angle measurement to mass resolution negligible already without primary vertex information

→ Good primary vertex selection needed for selection of signal jets

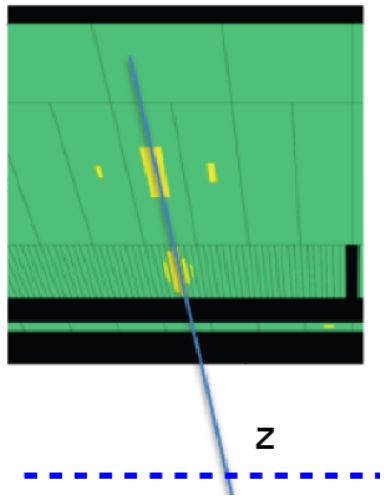

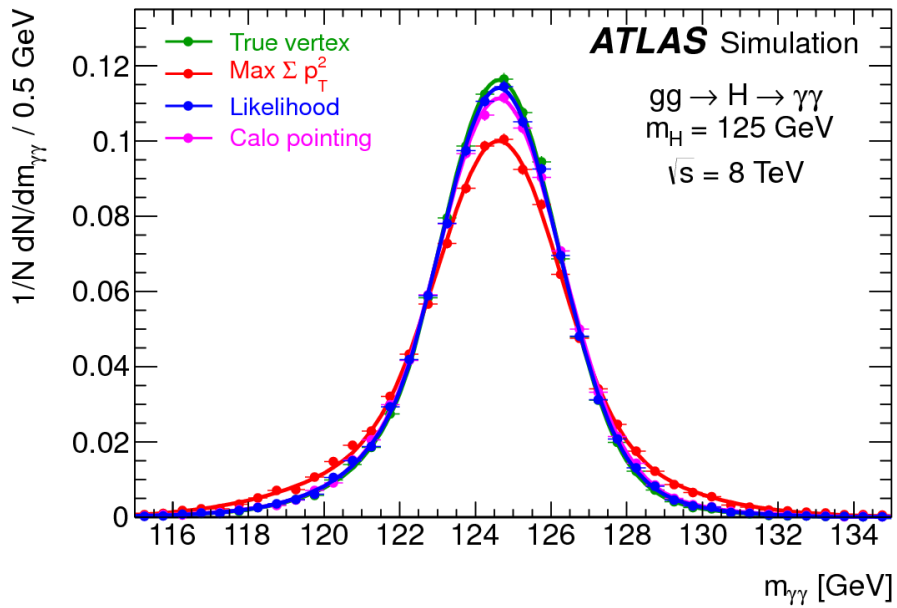

Photon pointing and primary vertex selection

$$m_{\gamma\gamma}^2 = 2E_1E_2(1-\cos\alpha)$$

Improve photon angle measurement using neural network ($8\,\mathrm{TeV}$) based on

- Photon pointing
  - ⋆ Photon direction measured from calorimeter using longitudinal segmentation
  - ⋆ Position of conversion vertex for converted photons (with Si hits)
- $\sum p_T^2$, $\sum p_T$ (over tracks) and angular balance in ϕ between tracks and diphoton system

→ Contribution of angle measurement to mass resolution negligible already without primary vertex information

→ Good primary vertex selection needed for selection of signal jets

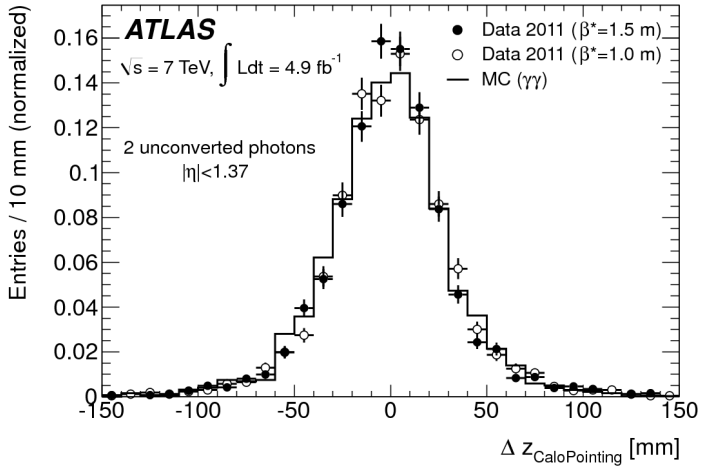

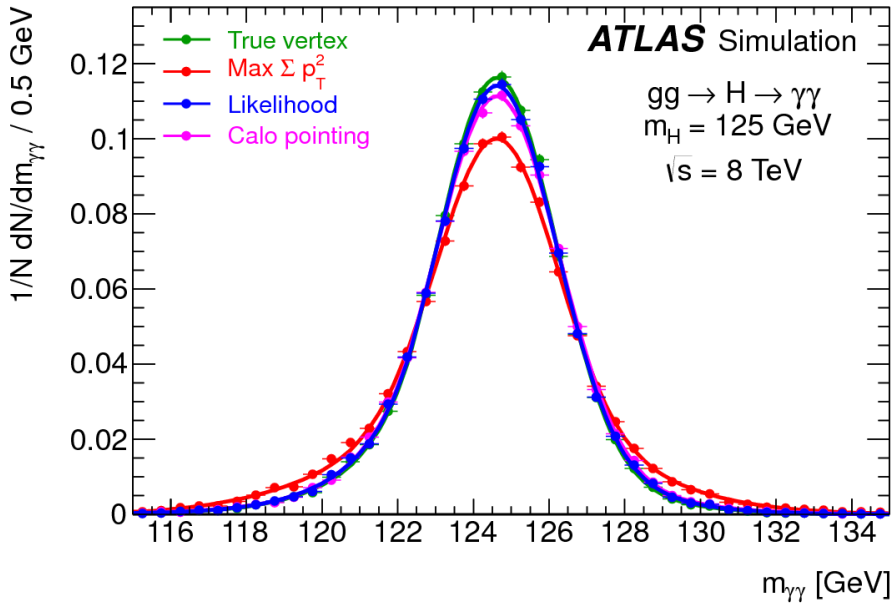

Photon pointing and primary vertex selection

$$m_{\gamma\gamma}^2 = 2E_1E_2(1-\cos\alpha)$$

Improve photon angle measurement using neural network ($8\,\mathrm{TeV}$) based on

- Photon pointing
  - ⋆ Photon direction measured from calorimeter using longitudinal segmentation
  - ⋆ Position of conversion vertex for converted photons (with Si hits)
- $\sum p_T^2$, $\sum p_T$ (over tracks) and angular balance in ϕ between tracks and diphoton system

→ Contribution of angle measurement to mass resolution negligible already without primary vertex information

→ Good primary vertex selection needed for selection of signal jets

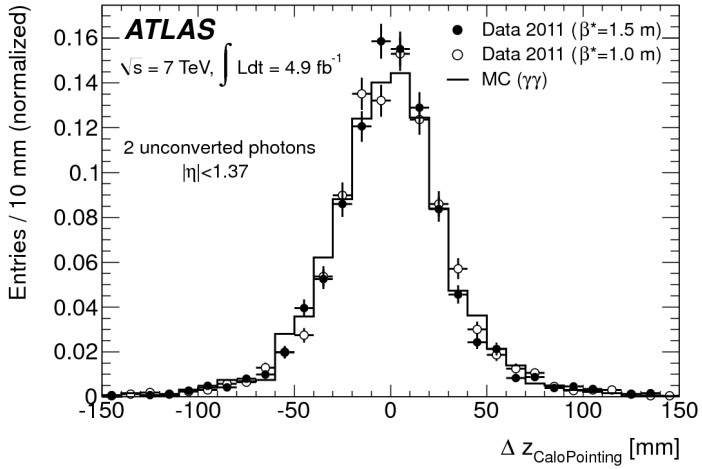

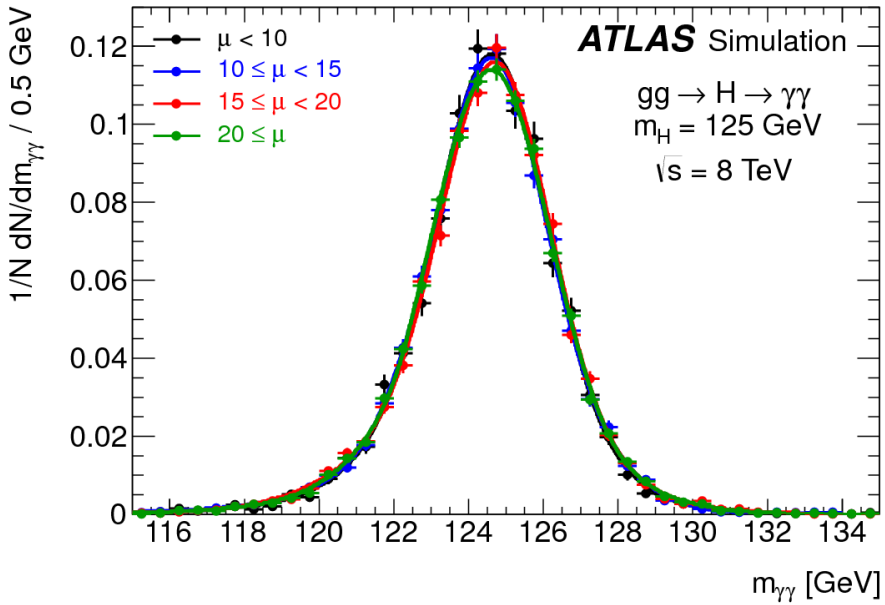

Categorization overview

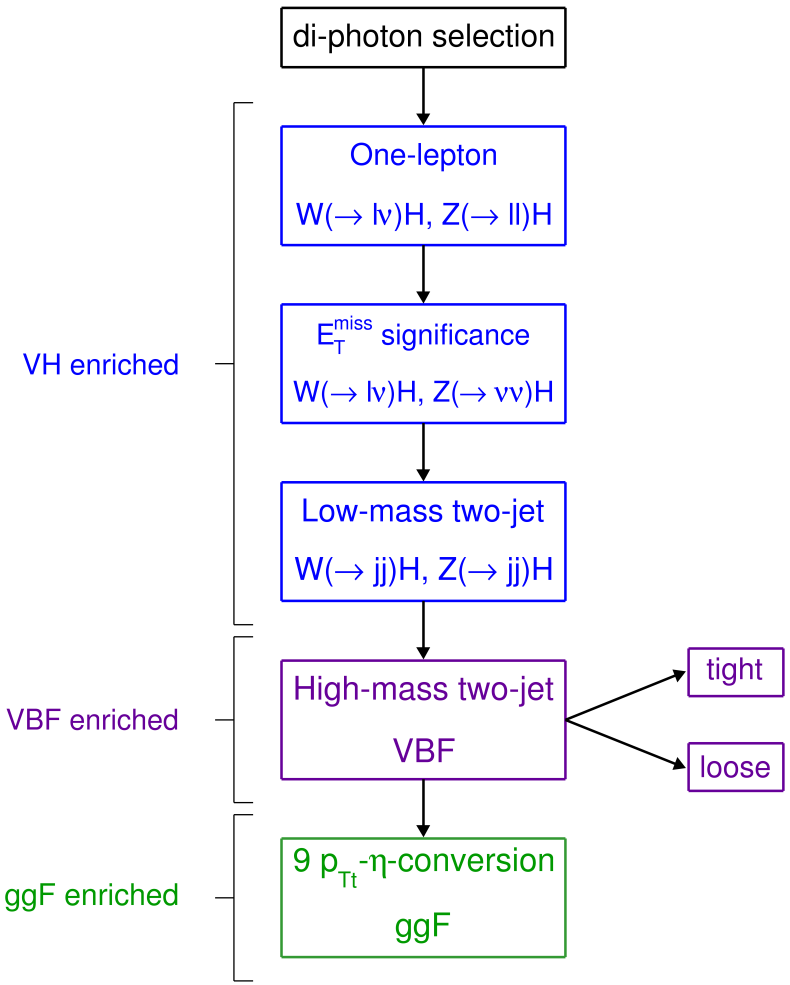

New categories for $\sqrt{s} = 8\,\mathrm{TeV}$

Diphoton selection

Identified and isolated photons
$p_T^{\gamma 1} > 40\,\mathrm{GeV}$, $p_T^{\gamma 2} > 30\,\mathrm{GeV}$

- Dedicated categories for separation of production processes
- Remaining events split into categories of varying signal resolution and S/B

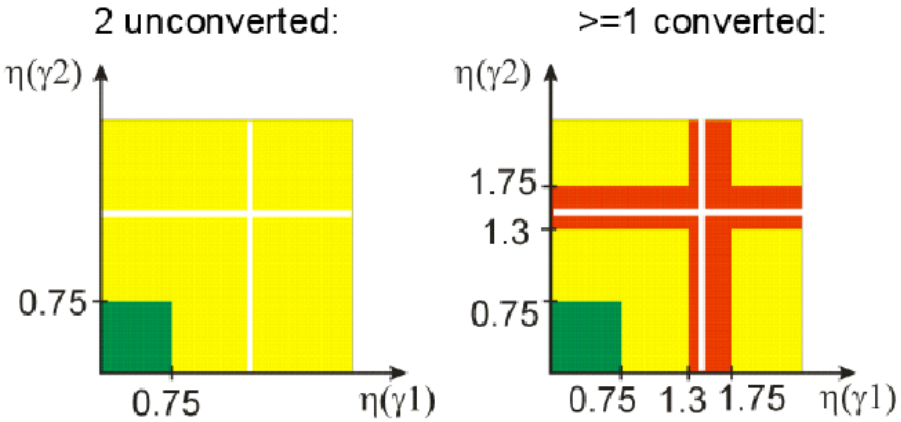

VBF-enriched categories

MVA-based selection for events with 2 jets (new)

- $\eta_{j1,2}$, $\Delta\eta_{jj}$, $p_{Tt}^{\gamma\gamma}$, $\Delta\phi_{\gamma\gamma;jj}$,
- $\eta^* = \eta_{\gamma\gamma} - 1/2(\eta_{j1} + \eta_{j2})$, $\Delta R_{\min}^{\gamma j}$

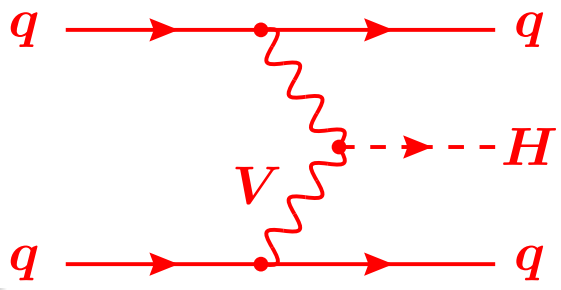

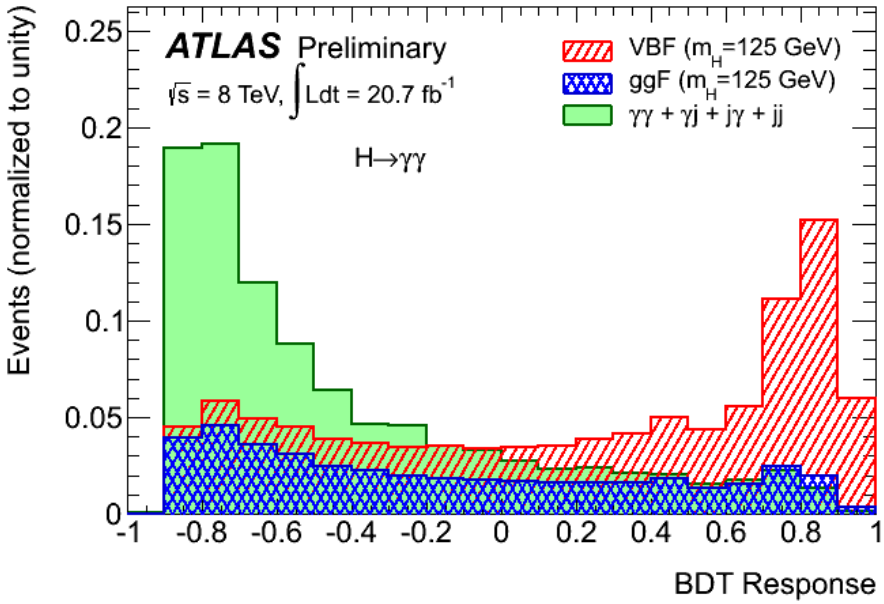

BDT trained to separate VBF from nonresonant background

- Also gives good separation from gluon fusion signal

	VBF purity	N_{sig}	cut
tight	76%	8.1	> 0.74
loose	54%	5.3	> 0.44

2-Jets candidate

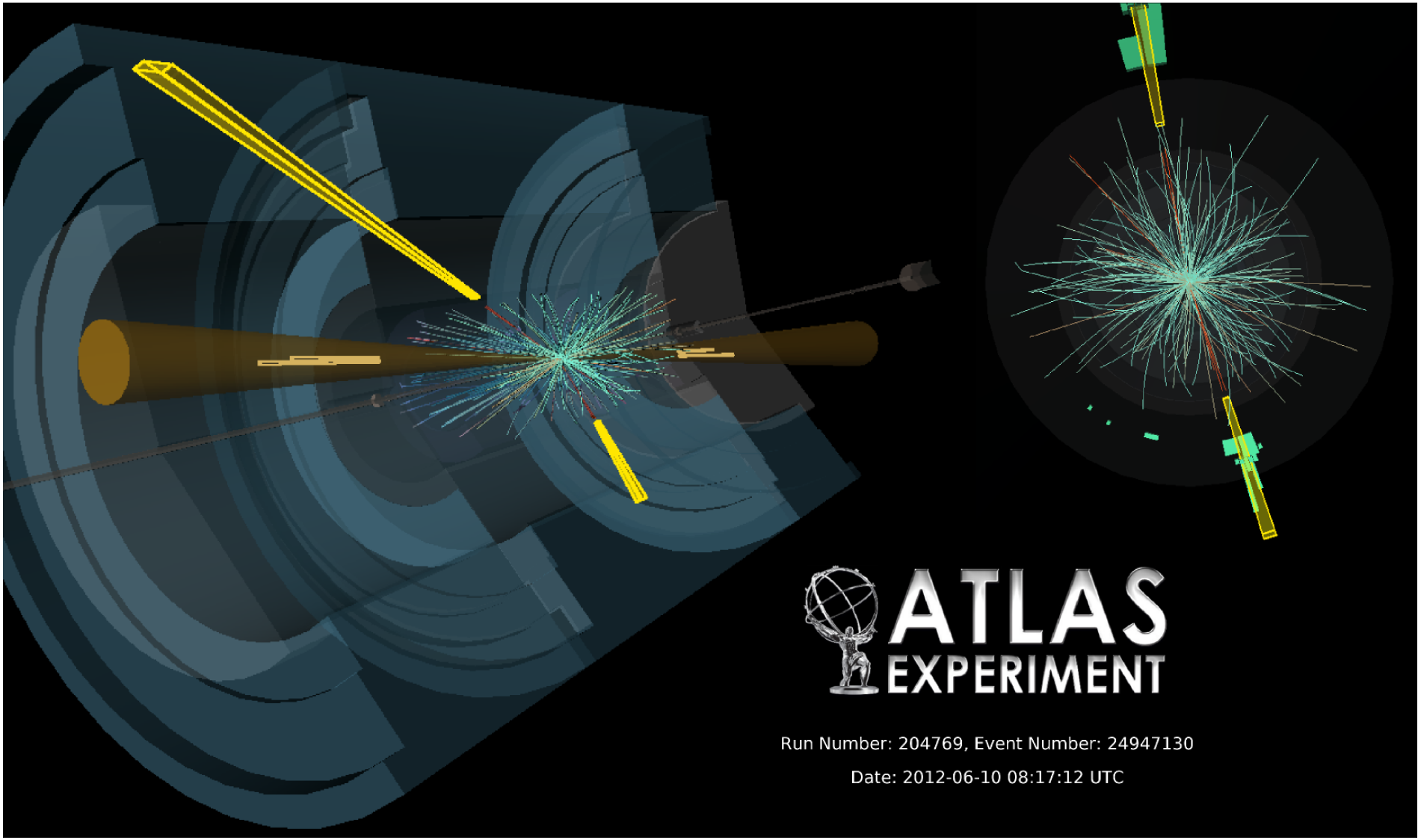

VH-enriched categories

Inclusive leptons ($W \to \ell\nu$, $Z \to \ell\ell$)

$p_T^e > 15\,\mathrm{GeV}$ or $p_T^\mu > 10\,\mathrm{GeV}$, isolated in tracker and calorimeter

Missing energy ($W \to \ell\nu$, $Z \to \nu\nu$) (new)

E_T^{miss} significance $\dfrac{E_T^{\mathrm{miss}}}{0.67 \sum E_T} > 5$

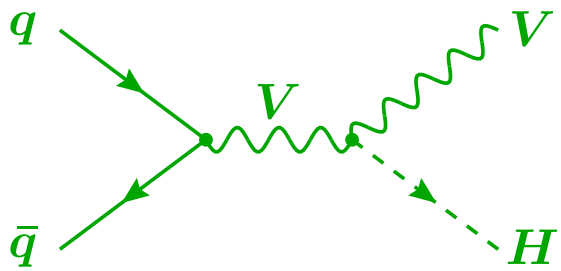

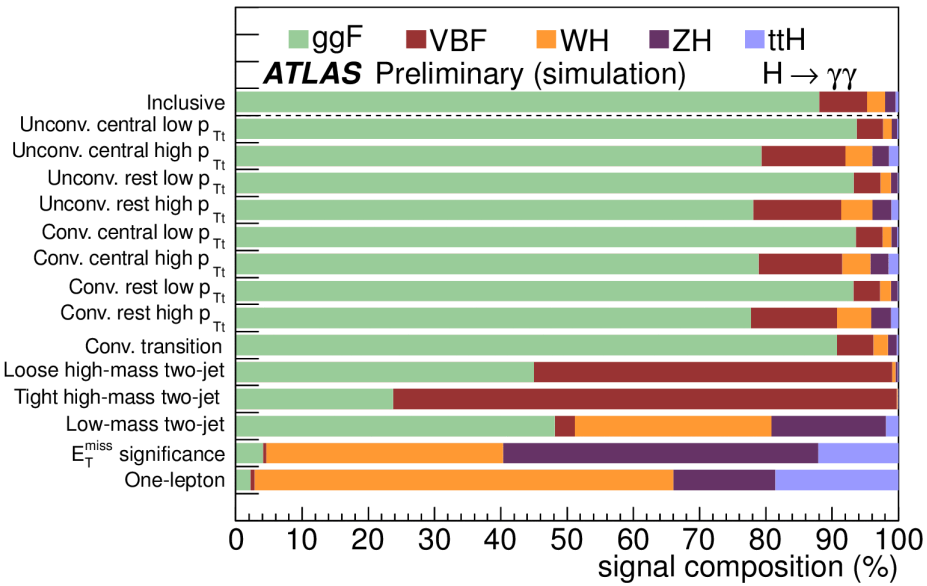

Dijet ($W \to jj$, $Z \to jj$)

$60\,\mathrm{GeV} < m_{jj} < 110\,\mathrm{GeV}$, $|\Delta\eta_{jj}| < 3.5$

	VH purity	N_{sig}
lepton	82%	2.9
E_T^{miss}	83%	1.3
dijet	47%	3.3

Mass spectrum and background parametrization

7 TeV + 8 TeV data (inclusive)

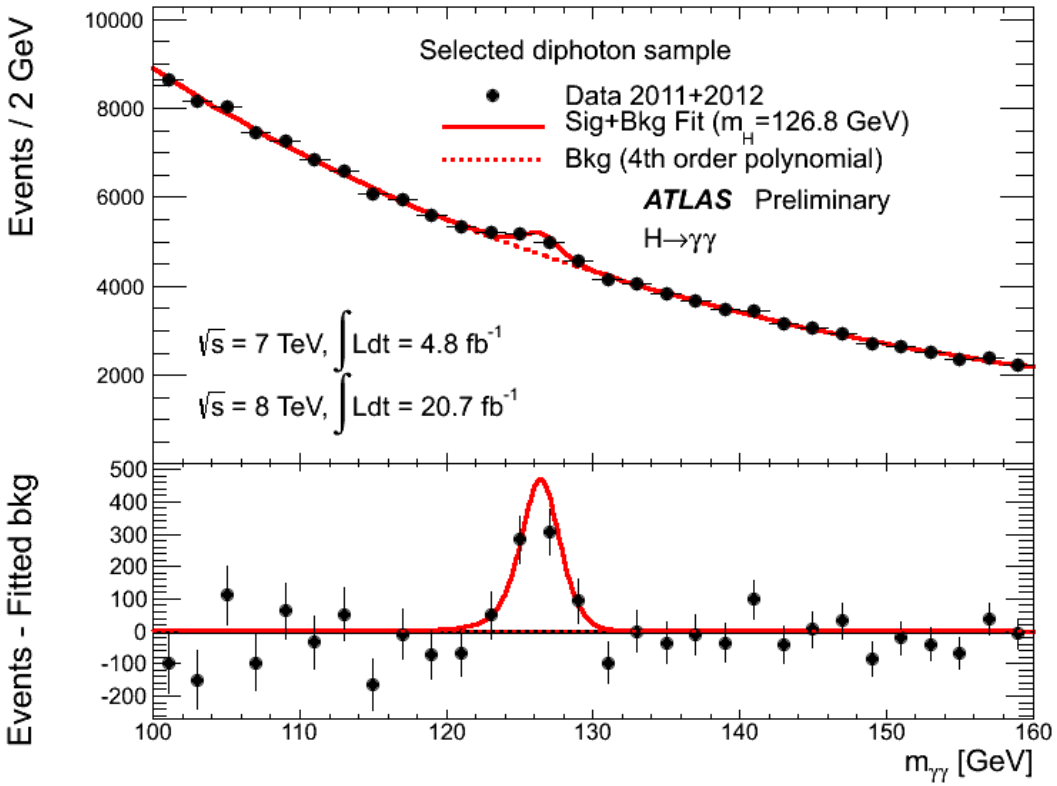

Background+signal fit, signal fixed at **126.8 GeV**

23788 events (**7 TeV**)
118893 events (**8 TeV**)

Background modelled by 4th order Bernstein polynomial, exponential of 2nd order polynomial, or exponential

Studied on high-statistics MC and chosen to give good statistical power while keeping potential biases acceptable

Potential bias accounted for as systematic uncertainty

A few category mass spectra

Unconverted central, high p_{Tt}

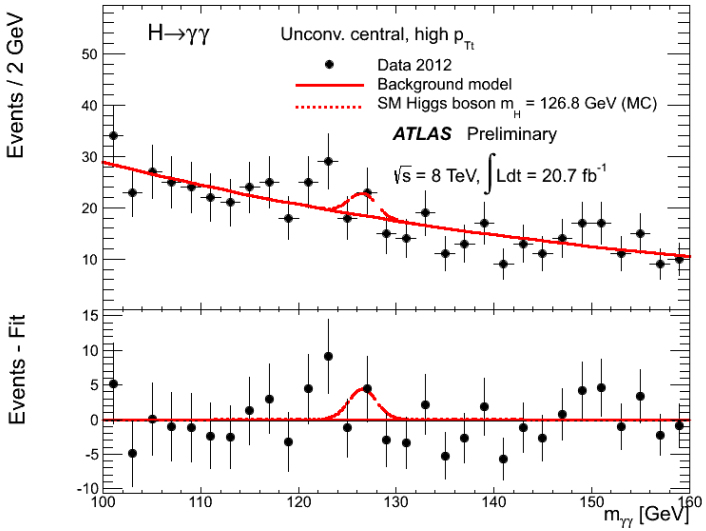

Converted rest, low p_{Tt}

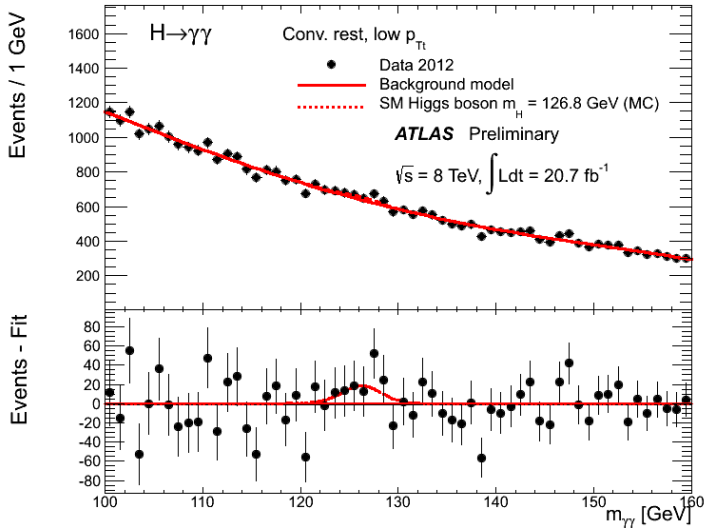

Tight high-mass 2-jet

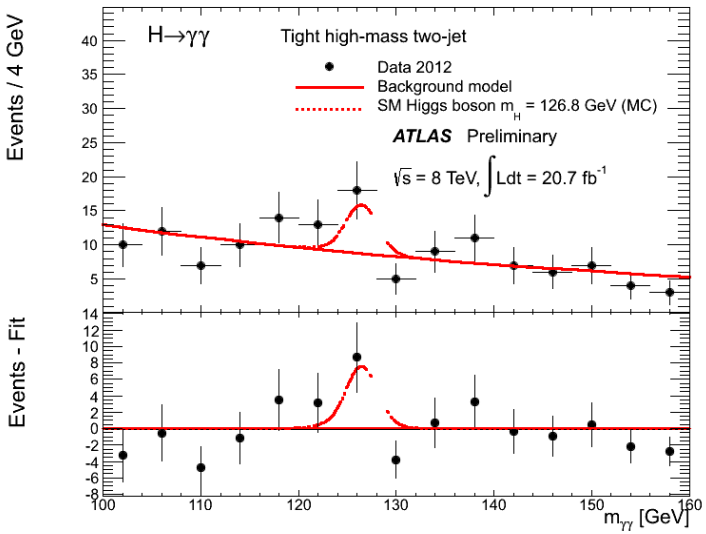

E_T^{miss} significance

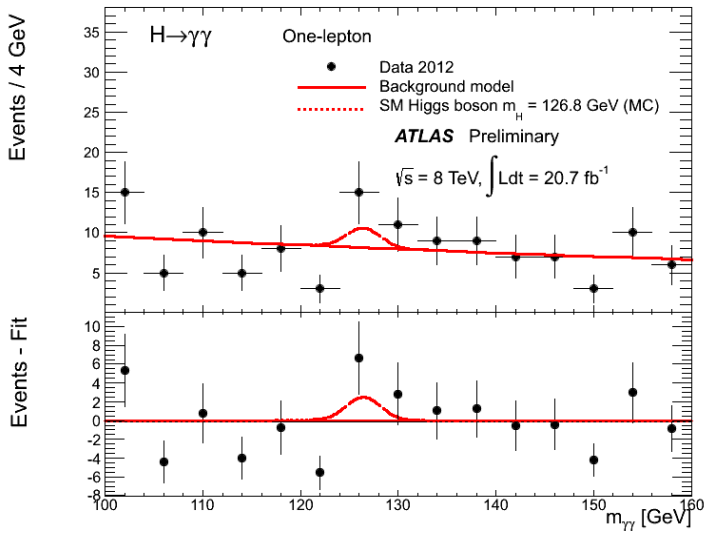

Main systematic uncertainties

	$\mathbf{7\ TeV}$	$\mathbf{8\ TeV}$
Photon id efficiency	8.4%	2.4%
Luminosity	1.8%	3.6%
Theory	up to 25%	up to 48%
	($gg \to H + 2$ jets)	
Jet E-scale (2-jets)	4-20%	
Underl. evt. (2-jets)	6-30%	2-13%
Higgs p_T	up to 12.5%	
Dijet modeling		up to 12%
Bkgd Param (evts)	0.2-4.6	0.1-11.4
$m_{\gamma\gamma}$ resolution	14%	14-23%
mass scale	0.6%	0.55%

Mass and signal strength

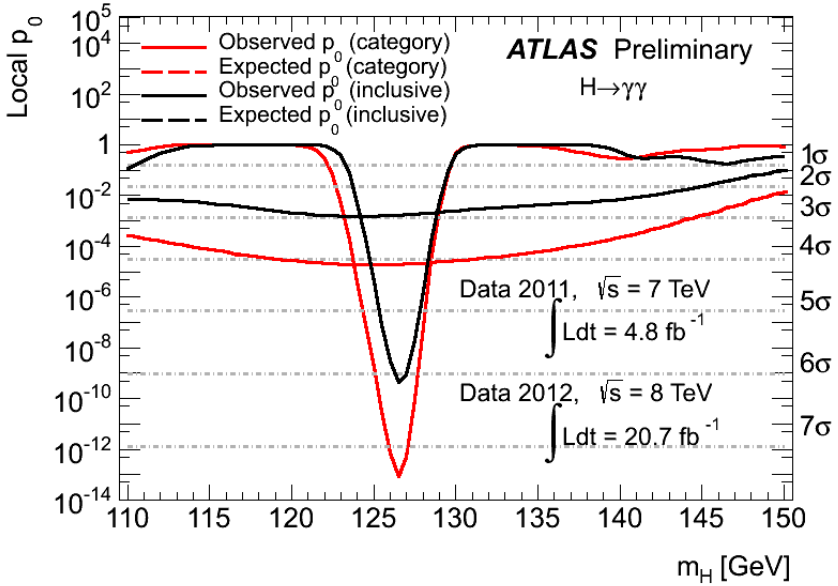

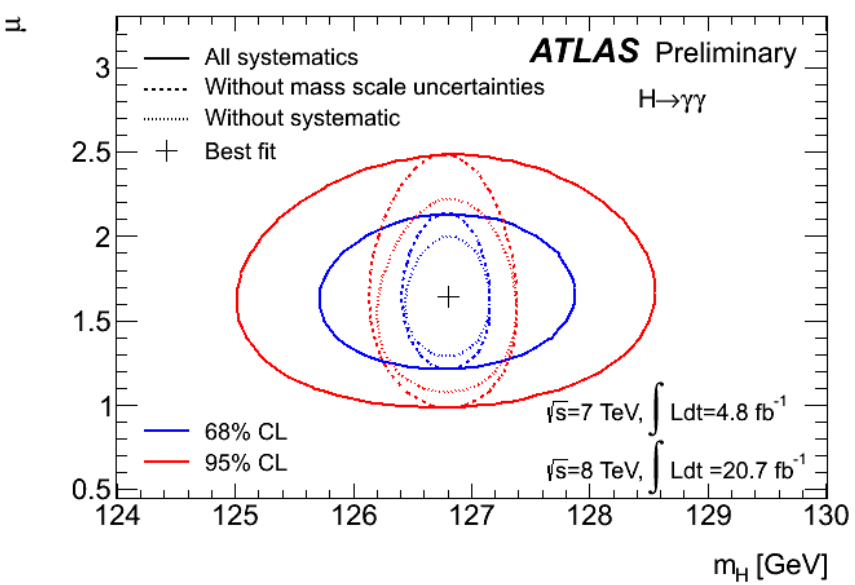

- Observed local significance of the excess $\mathbf{7.4}\,\boldsymbol{\sigma}$ ($\mathbf{4.1}\,\boldsymbol{\sigma}$ expected)
- Measured mass $\mathbf{126.8 \pm 0.2(stat) \pm 0.7(syst)\ GeV}$
- Measured signal strength $\boldsymbol{\mu = 1.65 \pm 0.24(\mathrm{stat})^{+0.25}_{-0.18}(\mathrm{syst})}$
  - ⋆ $\mathbf{2.3}\,\boldsymbol{\sigma}$ away from SM Higgs + background hypothesis
- Measured fiducial cross section (inclusive analysis)
  $\boldsymbol{\sigma_{\mathrm{fid}} \times BR = 56.2 \pm 10.5(\mathrm{stat}) \pm 6.5(\mathrm{syst}) \pm 2.0(\mathrm{lumi})\ \mathrm{fb}}$
  $(\boldsymbol{p_T^\gamma > 40, 30\ \mathrm{GeV}, |\eta^\gamma| < 2.37})$

Separating production processes

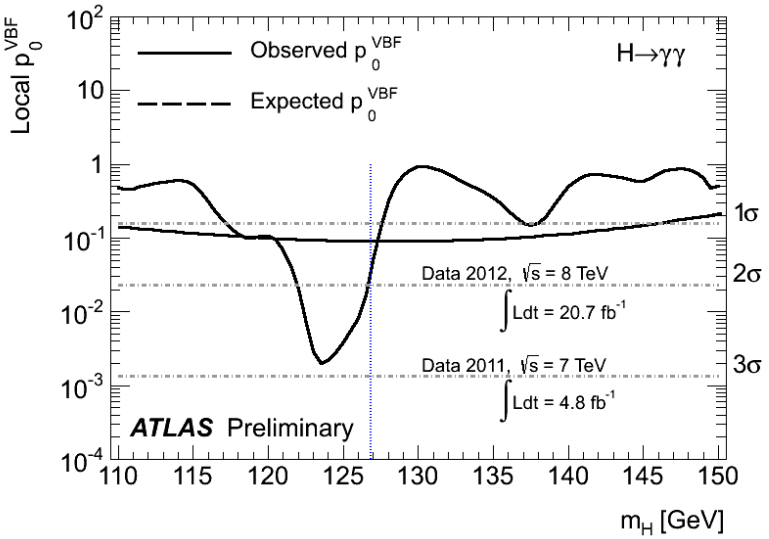

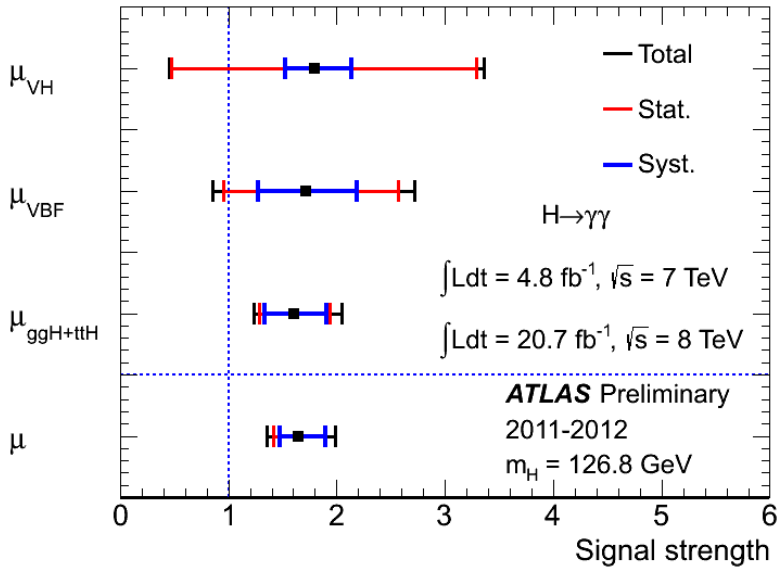

Searching for VBF signature

$\sim 2\,\sigma$ hint of VBF production

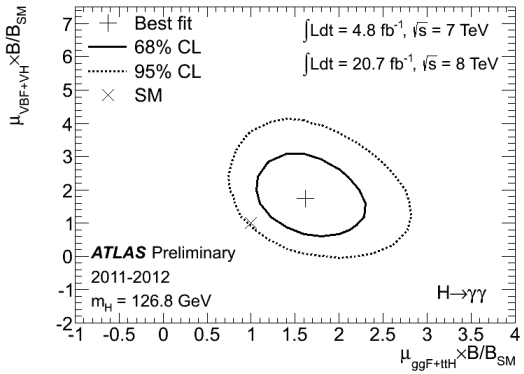

Signal strength per production process

$$\mu_{ggH+ttH} \times B/B_{\mathrm{SM}} = 1.6 \pm 0.3(\mathrm{stat})^{+0.3}_{-0.2}(\mathrm{syst})$$

$$\mu_{\mathrm{VBF}} \times B/B_{\mathrm{SM}} = 1.7 \pm 0.8(\mathrm{stat})^{+0.5}_{-0.4}(\mathrm{syst})$$

$$\mu_{VH} \times B/B_{\mathrm{SM}} = 1.8^{+1.5}_{-1.3}(\mathrm{stat})^{+0.3}_{-0.3}(\mathrm{syst})$$

Uncertainties on VBF and VH signal strengths improved by **30** and **45%**

Spin studies

Polar angle θ^* in resonance rest frame sensitive to spin of resonance

spin 0^+ $\mathrm{d}N/\mathrm{d}|\cos\theta^*| \sim$ const

spin 2^+ $\mathrm{d}N/\mathrm{d}|\cos\theta^*| \sim 1 + 6\cos^2\theta^* + \cos^4\theta^*$

(for spin 2 produced by gg fusion in minimal coupling model)

$\rightarrow$ strongly distorted by kinematic selection

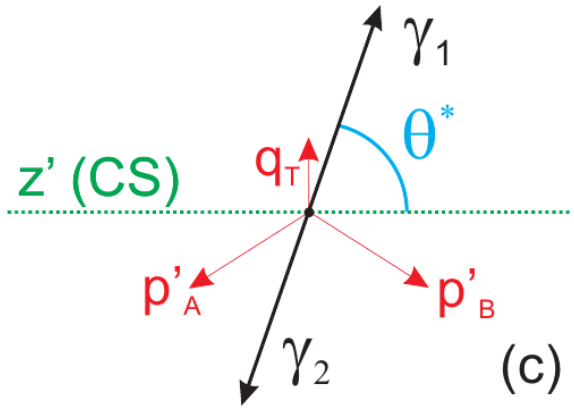

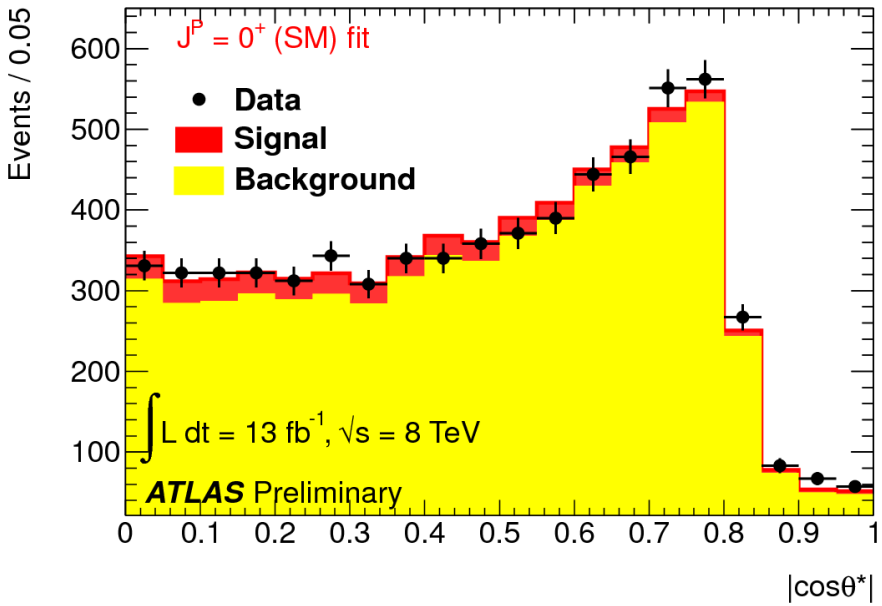

Background $|\cos\theta^*|$ shape interpolated from $m_{\gamma\gamma}$ sidebands into signal region (123.8 to $128.6\,\mathrm{GeV}$)

- Expect 199^{+34}_{-25} signal events (3% expected purity)

Analysis performed on $13\,\mathrm{fb}^{-1}$ of $\sqrt{s} = 8\,\mathrm{TeV}$ data

Spin studies

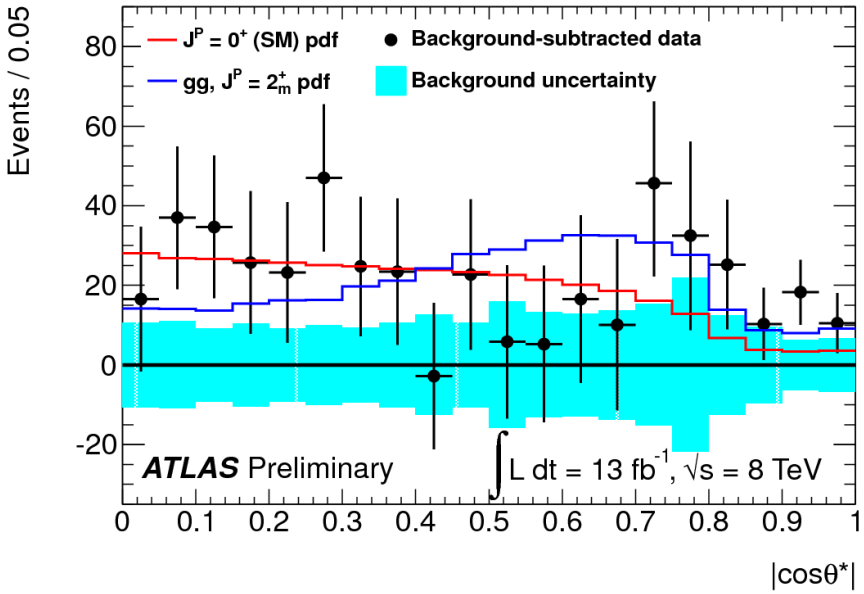

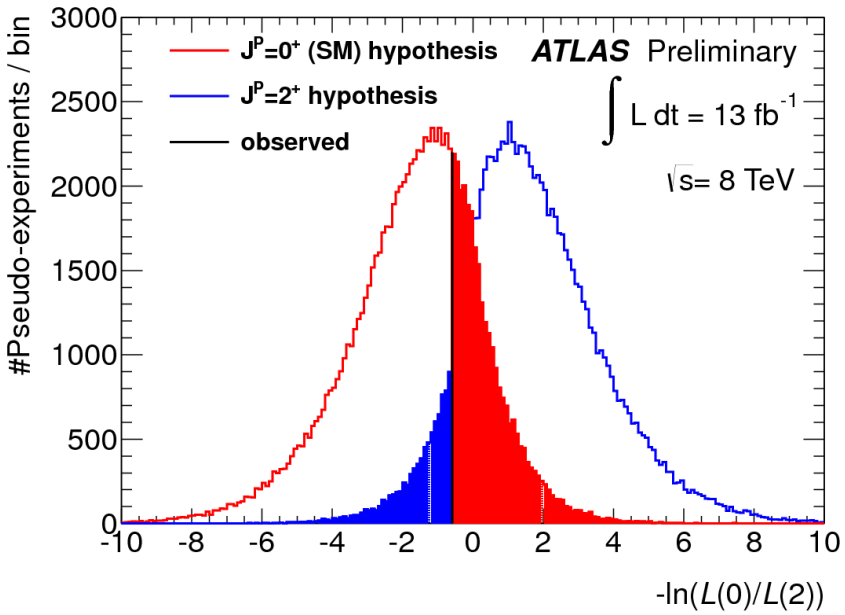

Compatibility of data with spin-0^+ signal plus background hypothesis and spin-2^+ signal plus background hypothesis estimated via likelihood ratio

$$q = -\mathbf{ln}\mathcal{L}(\mathbf{spin0}, \hat{\theta})/\mathbf{ln}\mathcal{L}(\mathbf{spin2}, \hat{\theta})$$

Expected spin 0 and spin 2 separation $\sim \mathbf{1.8}\,\boldsymbol{\sigma}$

Observed p-values $p_{2+} = 8.6\%$ and $p_{0+} = 29\%$

Spin 0 favored over tested spin 2 model

Summary

- New boson confirmed in $\gamma\gamma$ decay with $\mathbf{7.4\,\sigma}$
- Measured mass
  $\mathbf{126.8 \pm 0.2(stat) \pm 0.7(syst)\ GeV}$
- Measured signal strength
  $\mu = \mathbf{1.65 \pm 0.24(stat)^{+0.25}_{-0.18}(syst)}$
  - ⋆ $\mathbf{2.3\,\sigma}$ away from SM Higgs + background hypothesis
- Measured fiducial cross section $\sigma_{\mathbf{fid}} \times BR =$
  $\mathbf{56.2 \pm 10.5(stat) \pm 6.5(syst) \pm 2.0(lumi)\ fb}$
  - ⋆ Model independent
- Spin 0 somewhat favored over spin 2 (gg with minimal couplings)

See also talk by Jana Schaarschmidt in T49

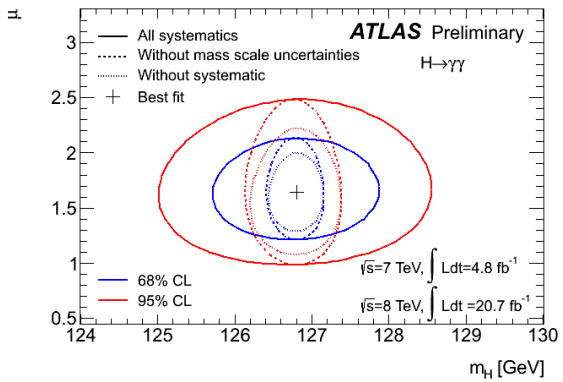

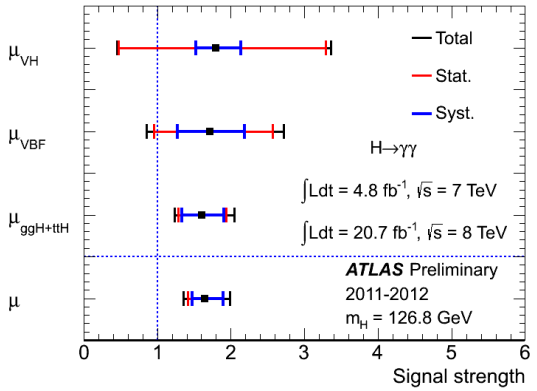

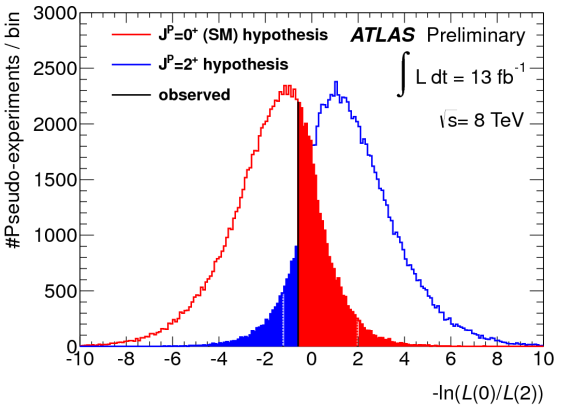

Backup

ATLAS Inner Detector (ID) and EM Calorimeter

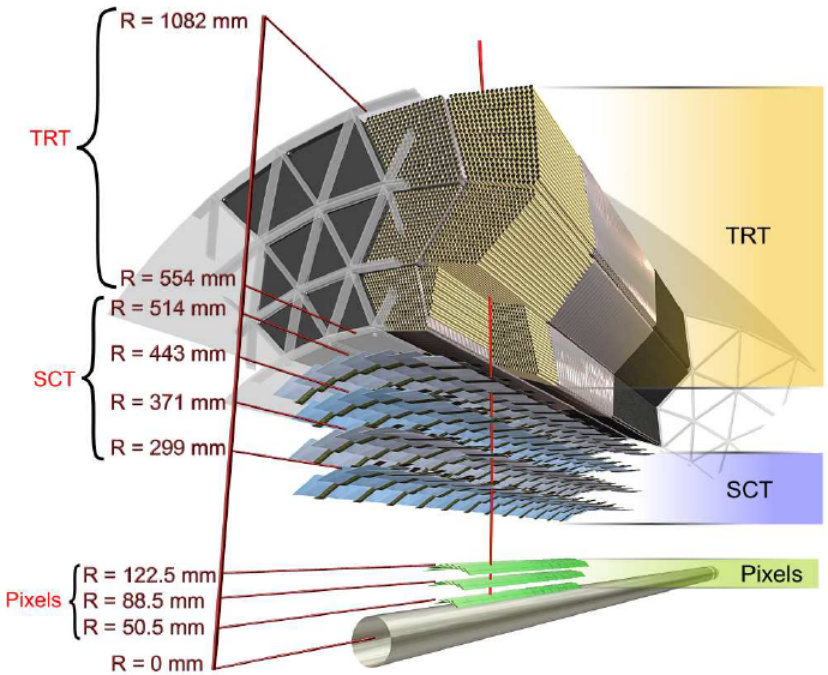

$|\eta| < 2.5$, barrel-endcaps geometry

- 3 layers Si Pixel
- 4 double layers Si strips (SCT)
- ~ 35 hits in Transition Radiation Tracker (TRT)
  - ⋆ $e^{\pm}$ identification capabilities through transition radiation

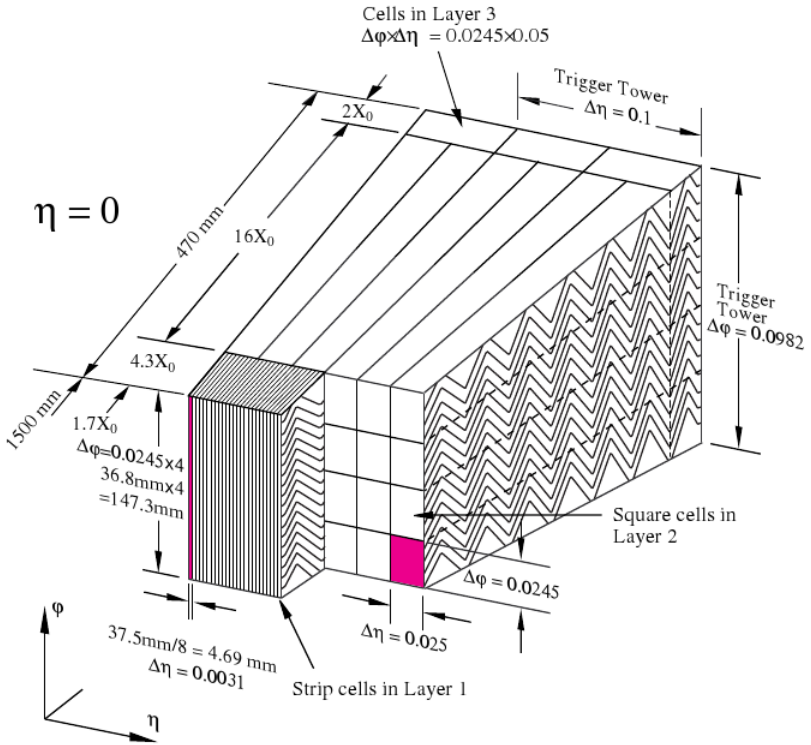

$|\eta| < 3.2$, barrel-endcaps geometry

- Pb-LAr sampling calorimeter
- 3 longitudinal layers with accordion geometry
- Presampler provides preshower sampling inside the cryostat